npj | clean water

Article

Published in partnership with King Fahd University of Petroleum & Minerals

https://doi.org/10.1038/s41545-025-00520-z

Enhanced degradation of triclosan using aerated hydrodynamic cavitation: turbulence-based modelling and economic evaluation

Mehdi Khiadani[1,2], Ensiyeh Taheri[1,3], Veena Bobade[1] & Ali Fatehizadeh[1] ✉

Pharmaceutical and personal care product (PPCP)-contaminated wastewater, particularly with triclosan (TCS), poses a significant environmental concern due to TCS persistence, ecotoxicity, and endocrine-disrupting effects, necessitating the development of efficient and sustainable remediation technologies. In this study, the degradation of TCS using hydrodynamic cavitation coupled with air injection (aerated HC process) is investigated as a green and chemical-free treatment method for wastewater treatment. Initially, the optimum operating conditions of the standalone HC process were determined by varying the inlet pressure and flow rate, which were found to be 2.34 bar and 0.45 L/s, respectively, corresponding to the highest turbulence frequency level of 1041 s^{-1} and the lowest turbulent pressure −0.58 bar at the venturi throat, based on the turbulence model. Subsequently, upon introducing an air flow rate of 1.6 m^3/h at the venturi throat, the aerated HC process achieved a TCS degradation efficiency of 79.89 ± 3.99%, with a synergistic index of 1.29 (compared to 71.54 ± 2.29% without air injection), confirming the enhanced performance due to air injection. The highest rate constant (0.073 min^{-1}) was observed at pH 3, confirming that acidic conditions favour TCS degradation. Mechanistically, TCS degradation in the aerated HC process proceeds through both radical pathways, primarily mediated by hydroxyl radicals, and non-radical pathways such as thermal pyrolysis.

Pharmaceuticals and personal care products (PPCPs) have become a growing environmental concern due to their widespread use in medicine, cosmetics, and hygiene products[1,2]. These compounds and their metabolites enter aquatic ecosystems through excretion, washing, and industrial discharge, making them among the most frequently detected pollutants[3]. Triclosan (5-chloro-2-(2,4-dichlorophenoxy) phenol, TCS) is a prominent compound, a chlorinated biphenyl ether used as an antimicrobial agent in products like toothpaste, mouthwash, soaps, and household cleaners[1,3]. Its extensive use leads to significant environmental release, primarily through domestic sewage entering wastewater treatment plants (WWTPs)[4], with concentrations in municipal wastewater reaching up to 14 mg/L[5]. TCS has been detected in human blood, urine, and breast milk, though its full health effects remain under study. Concerns include endocrine disruption, allergic reactions, and other adverse outcomes. TCS also poses ecological risks, showing toxicity towards algae, invertebrates, and fish[6].

Conventional domestic WWTPs are not generally designed to remove micropollutants completely. A significant proportion of PPCPs, including TCS, undergo partial removal during primary and secondary biological treatment, primarily through biodegradation and sorption to sludge. However, substantial quantities often persist in treated effluents due to their complex and persistent molecular structures[1,7]. For instance, studies have reported TCS removal efficiencies in conventional WWTPs ranging from approximately 58% to over 90%, with activated sludge processes generally achieving higher removal rates[8]. Despite this, the concentrations of effluent substances typically remain within the range of tens of ng/L to a few μg/L[2]. Operating at these lower concentrations has the potential to enhance the performance of subsequent treatment systems, for example, by achieving a higher percentage of removal due to more favourable kinetics. Moreover, treating lower concentrations may result in a substantial reduction in operational costs, as it may necessitate reduced energy input or a shorter

[1]School of Engineering, Edith Cowan University, Joondalup, WA, Australia. [2]Mineral Recovery Research Center (MRRC), School of Engineering, Edith Cowan University, Joondalup, WA, Australia. [3]Department of Environmental Health Engineering, School of Health, Isfahan University of Medical Sciences, Isfahan, Iran. ✉e-mail: fatehizadeh@gmail.com

treatment duration compared to treating the higher concentrations found in raw wastewater. As a result, there is a growing need for efficient and targeted degradation methods. Several techniques have been investigated for the removal of TCS, including chlorination, ozonation, photocatalysis, electrochemical oxidation, adsorption, membrane filtration, and biodegradation[6]. Advanced oxidation processes (AOPs) have gained significant attention in recent years for their effectiveness in degrading a wide range of organic pollutants, achieving removal efficiencies of up to 80%. Despite their proven performance, these methods face several limitations, particularly in developing countries, due to high infrastructure and operational costs ($10–450/m^3)[9]. Other drawbacks include the recurring expense of chemical inputs like hydrogen peroxide (H_2O_2), the high capital and energy demands of ozonation and electrooxidation systems, and the formation of potentially toxic by-products during ozonation[2,10]. Additional challenges involve variable reagent dosing, low mineralisation rates, and short operational lifespans due to saturation in processes such as membrane filtration and the use of zero-valent iron particles[9]. Therefore, to address TCS contamination effectively—particularly in industrial contexts—there is a critical need to develop sustainable, efficient, and cost-effective treatment strategies[11].

Cavitation has emerged as a promising technique for wastewater treatment due to its ability to generate highly reactive free radicals, similar to AOPs[12]. It involves the rapid formation, growth, and collapse of microbubbles in a liquid medium, creating localised high-temperature and high-pressure conditions that lead to the dissociation of water molecules and the formation of oxidative species such as hydroxyl radicals (•OH), which drive pollutant degradation[13,14]. Cavitation can be classified into two types: acoustic cavitation, produced by ultrasound waves, and hydrodynamic cavitation (HC), generated by pressure variations in flowing liquids through constrictions[15]. The extreme conditions during bubble collapse (~10,000 K temperature and ~1000–5000 bar pressure) enhance the oxidation of organic contaminants via the generation of hydroxyl (•OH) radicals[16]. HC is particularly energy-efficient, consuming only 0.1–1 kWh/m^3—lower than photocatalysis (0.1–5 kWh/m^3), ozonation (0.2–2 kWh/m^3), and electrochemical oxidation (0.5–20 kWh/m^3)[17]. Moreover, for the same energy input, HC can treat twice the volume of wastewater compared to ozonation and three times more than photocatalysis[18,19].

Generally, combining HC with specific additives improves pollutant oxidation by enhancing the generation of reactive species and improving mixing. These additives include chemical oxidants like H_2O_2[20], ozone and air[21], persulfate, hypochlorite[12], peroxymonosulfate[17], and periodate[22]; catalysts or activators such as ferrous sulphate[20], carbon tetrachloride[13], zero-valent iron[23], and oxalic acid[22]; and physical enhancements like ultraviolet light[24], photocatalysis[25], plasma[26], acoustic cavitation[27], which often work synergistically with HC. Despite these advances, a substantial research gap persists in the development of a genuinely chemical-free, cost-effective, and highly efficient method for enhancing HC. A plethora of extant strategies, while efficacious, depend on the utilisation of costly chemical additives or energy-intensive physical processes. These processes have the potential to introduce secondary pollution risks and limit their feasibility, particularly in developing economies. In this context, the potential of aeration alone, a cost-free and widely accessible oxidant, to enhance cavitation efficiency has been the subject of only a limited amount of research, particularly in terms of the removal of PPCPs such as TCS. This assertion is particularly valid for systems operating at low inlet pressures, a condition that has the potential to enhance energy efficiency and reduce treatment costs. Moreover, there is an absence of systematic evaluations that integrate performance analysis, mechanistic insights via flow modelling, and economic viability.

This study directly addresses this gap by proposing and evaluating a new approach, including the use of air injection to intensify the HC process, to establish a green, chemical-free treatment method. The degradation of TCS was investigated under both conventional HC and aerated HC conditions at relatively low inlet pressures. Experiments were conducted using synthetically prepared water, thereby enabling precise control over the studied parameters, including pH, air flow rate, and initial TCS concentration. This controlled configuration facilitated a clear interpretation of the effects of individual variables on treatment efficacy. Despite the utilisation of synthetic water, the findings are pertinent to both raw and treated wastewater matrices, where residual TCS frequently persists due to insufficient removal by conventional treatment systems. The results, therefore, support the potential application of aerated HC as a polishing step or as an enhancement to existing treatment processes. In order to provide further elucidation on the mechanisms underpinning this phenomenon, a turbulence-based model was employed to simulate cavitation behaviour, thereby facilitating an understanding of the interplay between fluid dynamics and radical generation. A cost analysis was also undertaken to offer practical insight into the process scalability and economic viability. Subsequent research will concentrate on validating the process using real wastewater, where matrix complexity and the presence of competing constituents may influence degradation efficiency.

Results and discussion

Effect of inlet pressure and flow rate

As highlighted in the literature, inlet pressure and flow rate constitute key parameters influencing the performance of the HC process. To systematically investigate their effects on TCS degradation, experiments were conducted by varying the flow rate from 0.05 to 0.50 L/s at a low inlet pressure of 1.15 ± 0.09 bar, and from 0.05 to 0.45 L/s at a high inlet pressure of 2.76 ± 0.33 bar. The variation in TCS degradation efficiency under these differing inlet pressures and flow rates is illustrated in Fig. 1. The results indicate that both inlet pressure and flow rate significantly influence TCS degradation efficiency, with a general trend of enhanced degradation at higher operating conditions. When comparing the effect of inlet pressure at the same flow rates, increasing the pressure from the 1.15 ± 0.09 bar to 2.76 ± 0.33 bar led to an improvement in TCS degradation from 39.46 ± 2.17% to 44.11 ± 2.21% at a flow rate of 0.05 L/s, and from 61.29 ± 2.51% to 62.70 ± 3.14% at a flow rate of 0.25 L/s. Although the effect of inlet pressure diminishes at higher flow rates, the overall trend supports the role of inlet pressure in enhancing degradation under lower flow conditions. As evidenced in the literature[28], inlet pressure is pivotal in establishing the oxidative potential of HC systems, primarily by dictating bubble formation and collapse dynamics. Increasing the inlet pressure enhances the energy input per unit mass of liquid, fostering greater turbulence and a larger pressure drop across the cavitation device. This cascade of effects intensifies cavitation by increasing both the number and collapse strength of cavitation bubbles. The resultant elevated cavitation intensity generates more extreme localised environments (e.g. higher temperatures and pressures), which in turn promote the formation of a greater quantity of reactive free radicals[29]. During the passage of the aqueous solution through the venturi device and exposure to high and low pressures, the dissociation of water molecules occurs, leading to the formation of hydroxyl (•OH) radicals (Eq. 1)[30]. These radicals then drive non-selective oxidative reactions, ultimately accelerating the degradation of TCS.

$$H_2O \xrightarrow{HC} H^{\bullet} + {}^{\bullet}OH \quad (1)$$

The cavitation number (C_v), a dimensionless parameter quantifying the cavitation potential within the system, was used to evaluate the hydraulic characteristics of the venturi device. The values C_v were calculated according to Eq. (2), considering the fully recovered pressure downstream of the venturi (P_2, in Pa), the vapour pressure of the fluid at the operating temperature (P_v, in Pa), the liquid velocity at the venturi throat (v_{th}, in m/s), and the density of the reaction liquid (ρ, in kg/m^3)[23]. Figure 1c, d illustrates the calculated C_v values for the low and high inlet pressure conditions. As shown, the C_v decreased with increasing inlet pressure, a finding that aligns with previous research[31,32]. It is well-established that higher C_v values correspond to a lower cavitation potential, whereas lower C_v values indicate

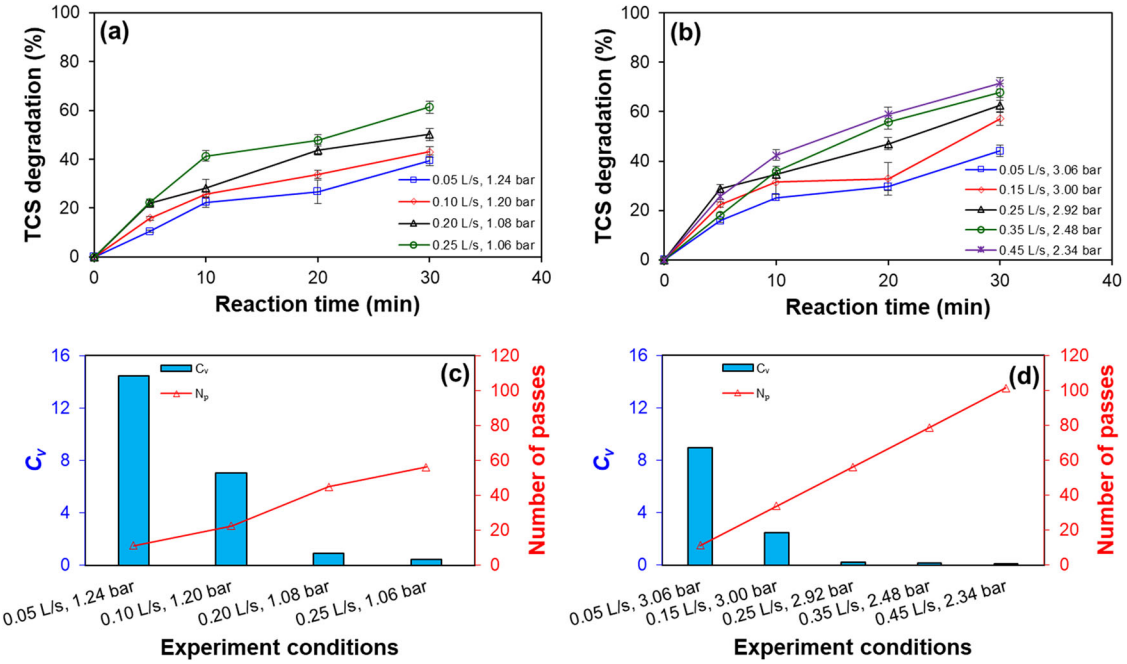

Fig. 1 | Variation of TCS degradation by HC process under various inlet pressure and flow rate. a Low inlet pressure and **b** high inlet pressure (Experimental condition: TCS concentration = 5 mg/L, solution pH = 7, and reaction time = 5–30 min), and cavitation and number of passes, **c** low inlet pressure, and **d** high inlet pressure.

more favourable cavitation conditions. Therefore, the observed decrease in C_v with increasing inlet pressure results in an increased number of cavities generated per unit time and volume, ultimately leading to improved degradation efficiency of the target organic pollutant. Theoretically, cavitation is expected to occur when the C_v is below 1.0 under ideal conditions[20]. However, in real-world applications, cavitation can also be observed at C_v values exceeding 1. This deviation from the ideal can be attributed to the presence of dissolved gases and suspended particles within the liquid. These impurities act as additional nucleation sites, facilitating the formation of cavitation bubbles even when the theoretical C_v threshold is not met[23,32]. This phenomenon explains the observed TCS degradation at C_v values greater than 1 in our experiments. Chen et al.[33] investigated the degradation of atrazine using an HC process with a venturi tube. Their study reported calculated C_v of 2.45, 2.20, and 2.16, corresponding to inlet pressures of 0.12 MPa, 0.15 MPa, and 0.17 MPa, respectively. The highest atrazine degradation was observed at 0.15 MPa ($C_v = 2.20$), suggesting that an optimal C_v value can result in strong cavitation intensity and a significant amount of reactive oxygen species.

$$C_v = \frac{P_2 - P_v}{0.5\rho v_{th}^2} \tag{2}$$

In another aspect, flow rate significantly influenced TCS degradation in the HC process at both low and high inlet pressures. Increasing the flow rate from 0.05 to 0.25 L/s at low inlet pressure resulted in a substantial increase in TCS degradation efficiency from 39.46 ± 2.17% to 61.29 ± 2.51%. Moreover, at high inlet pressure, raising the flow rate from 0.05 to 0.45 L/s improved TCS degradation efficiency from 44.11 ± 1.89% to 71.54 ± 2.29%. To evaluate the residence time of TCS under cavitation conditions, the number of passes (N_p) was calculated using Eq. (3)[34], where Q is the flow rate through the mainline (L/s), t is the degradation time (s), and V is the total volume of the reaction liquid (L). As expected, a higher flow rate resulted in a greater N_p and, consequently, higher degradation efficiency. This enhancement likely results from the increased number of passes through the venturi per unit time at higher flow rates, leading to increased cumulative exposure of TCS within the active cavitation region and more frequent exposure to the intense conditions. Given that pyrolysis within the collapsing cavitation bubbles is a key degradation mechanism in HC[23], the increased throughput facilitates more effective thermal decomposition of TCS, thus improving overall degradation efficiency.

$$N_p = \frac{Qt}{V} \tag{3}$$

It is worth noting that, based on the performance curve of the centrifugal pump (Fig. S1), an increase in inlet pressure resulted in a corresponding decrease in flow rate, and vice versa. Both inlet pressure and flow rate are critical parameters influencing the C_v and N_p, which are essential in characterising the HC process behaviour. These findings collectively underscore the importance of hydrodynamic conditions in optimising the HC process for wastewater treatment applications. Generally, elevated inlet pressures and flow rates enhance cavitation intensity by promoting stronger bubble formation and collapse, as reflected by lower C_v values. This, in turn, contributes to more effective TCS degradation. Understanding the interplay between these parameters allows operators to fine-tune system conditions for maximum cavitation efficiency, thereby improving pollutant removal performance and overall process effectiveness using the HC process.

To provide deeper insights into the cavitation phenomena occurring in an HC process equipped with a circular venturi, turbulence-based modelling can be employed. This approach enables detailed analysis of the complex, unsteady flow structures and pressure fluctuations within the cavitation reactor, which are critical for bubble formation and collapse dynamics[35,36]. As the liquid flows through the venturi, the reduction in cross-sectional area leads to an increase in velocity head at the expense of pressure head, in accordance with Bernoulli's principle. This localised drop in pressure at the venturi throat creates favourable conditions for cavitation inception. The dynamics of cavity clusters generated in this region are closely governed by the surrounding pressure field. In turbulent flow through the venturi, pressure fluctuations are influenced by velocity fluctuations caused by the formation of eddies. These eddies induce localised variations in pressure, which in turn affect bubble formation, growth, and collapse. The instantaneous velocity in the flow direction (x-axis), denoted as v_x, can be decomposed into the sum of the averaged velocity ($\overline{v}_x$) at a given point along the x-direction (m/s) and the fluctuating velocity component (v'), as described by Eq. (4). Analogous decompositions can be formulated for the velocity components in the y

and z directions. Furthermore, the turbulent kinetic energy per unit mass of the liquid ($K.E$) can be calculated using Eq. (5). Based on this, the rate of dissipation of turbulent kinetic energy per unit mass of the liquid (P_M), representing the loss of kinetic energy due to turbulence, was computed using Eq. (6). Assuming isotropic turbulence, where the root-mean-square fluctuating velocities are approximately equal in all direction($v'_x \approx v'_y \approx v'_z \approx v'$), Eq. (6) can be reduced to Eq. (7).

$$v_x = \bar{v}_x + v' \tag{4}$$

$$K.E = \frac{1}{2}[(v'_x)^2 + (v'_y)^2 + (v'_z)^2] \tag{5}$$

$$P_M = -\frac{1}{2}\frac{d}{dt}[(v'_x)^2 + (v'_y)^2 + (v'_z)^2] \tag{6}$$

$$P_M = -\frac{3}{2}\frac{d}{dt}(v')^2 \tag{7}$$

In the context of isotropic turbulence, the v' and the characteristic length scale of the energy-containing eddies (l) are intrinsically related to the dissipation of turbulent kinetic energy (P_M), as expressed in Eq. (8). These parameters play a crucial role in governing the dynamics of turbulent flows. Specifically, the frequency of turbulent velocity fluctuations (f_T) is directly influenced by l and can be approximated as being inversely proportional to l, as shown in Eq. (9). According to Prandtl's mixing length theory, the l can be estimated using Eq. (10), where d_x represents the local diameter of the venturi tube at the position of the cavity cluster at any given time. Downstream of the venturi throat, the expanding section facilitates pressure recovery. The fluid cluster's trajectory in this region can be estimated using its exit velocity and throat dimensions (Eq. 11). The divergence angle (α) of the venturi, defined in Eq. (12), characterises the geometry of the pressure recovery zone (x) and influences cavitation dynamics, where d_p and d_{th} are the diameter of the pipe and venturi throat, L is length of the expansion section of the venturi.

$$P_M = \frac{(v')^3}{l} \tag{8}$$

$$f_T = \frac{v'}{l} \tag{9}$$

$$l = 0.08 d_x \tag{10}$$

$$d_x = (2x\alpha) + d_{th} \tag{11}$$

$$\alpha = \frac{d_p - d_{th}}{2L} \tag{12}$$

Lastly, based on the modified Bernoulli's equation for turbulent flow, turbulent pressure (P_x) was computed using Eq. (13), where P_{th} is liquid pressure at the venturi throat, v_{tn} is velocity of the liquid at any point downstream of the venturi, ΔP is permanent pressure drops, and V_V and $V_{V,I}$ are total volume of the expansion section of venturi and volume of the expansion section of venturi at any point in the x-direction, respectively. In Eq. (13), v_{tn}, shape-dependent Scherrer's constant (k), and ΔP were calculated via Eqs. (14)–(16), respectively. The friction factor (f_r), related to the Reynolds number (N_{Re}), was estimated for turbulent flow conditions using Eq. (17).

$$P_x = P_{th} + \tfrac{1}{2}\rho\left(v_{th}^2 - v_{tn}^2\right) - \left[\Delta P\left(\frac{V_{V,i}}{V_V}\right) - k\left[\Delta P\left(\frac{V_{V,i}}{V_V}\right)\right]^{2/3}\right] \tag{13}$$

$$v_{tn} = v_t + v'(\sin(2\pi f_T t)) \tag{14}$$

$$k = \frac{1}{2}\rho^{1/3}\left(\frac{Q}{V_V}l\right)^{2/3} \tag{15}$$

$$\Delta P = \frac{4 f_r L v_t^2 \rho}{d_p} \tag{16}$$

$$f_r = \frac{0.079}{N_{Re}^{0.25}} \tag{17}$$

Figure 2 presents a graphical representation of the turbulence model along the normalised axial distance (x/L) of the venturi for various inlet pressures and flow rates. Overall, increasing the inlet pressure and flow rate led to an enhancement in the turbulence frequency, the rate of dissipation of turbulent kinetic energy, and the turbulent pressure downstream of the venturi device. Specifically, the dissipation rate of turbulent kinetic energy was highest near the venturi throat, reaching a maximum value of 1627 Pa observed at an inlet pressure of 2.34 bar and a flow rate of 0.45 L/s (Fig. 2a,b). This elevated dissipation rate contributes to the formation of a greater number of cavitation bubbles, subsequently leading to improved degradation efficiency of the target molecules. Furthermore, the highest turbulence frequency (1041 s^{-1}) was observed at a flow rate of 0.45 L/s and an inlet pressure of 2.34 bar, while the lowest frequency (139 s^{-1}) occurred at a flow rate of 0.05 L/s and an inlet pressure of 1.24 bar (Fig. 2c,d). This finding clearly demonstrates the direct impact of both flow rate and inlet pressure on the turbulence characteristics within the HC system. As shown in Fig. 2e,f, the gradient of turbulent pressure across the venturi expanded with increasing inlet pressure and flow rate. At the venturi throat, the turbulent pressure decreased from 3.03 bar to −0.58 bar at high inlet pressure and from 1.23 bar to 0.14 bar at low inlet pressure. This intensified pressure gradient enhances bubble collapse due to higher turbulence-induced stresses, ultimately improving the overall efficiency of the HC process.

It is important to note that, according to Bernoulli's principle, the energy input to the HC process depends on both pressure and flow rate, with pump power approximately proportional to their product. Given the interdependence between pressure and flow rate in centrifugal pumps (Fig. S1), optimising turbulent pressure gradients requires prioritising flow rate over inlet pressure. High inlet pressures demand larger pumps, which increase electricity consumption and operational costs. Therefore, balancing these parameters is essential for efficient HC process design. These findings highlight the critical role of flow rate and pressure in shaping turbulence and pressure gradients within venturi-based HC processes. A well-optimised balance enhances performance while minimising energy use and treatment costs.

Effect of air injection

This study also aimed to enhance the performance of the HC process by integrating air injection as a low-cost and readily available enhancement method. To achieve this, air was injected into the throat of the venturi device at various flow rates, while maintaining a constant TCS concentration (5 mg/L) and a solution pH of 7. Figure 3a illustrates the variation in TCS degradation achieved by the aerated HC process under these different air flow rates. As illustrated, TCS degradation exhibited a significant dependence on the air flow rate. In the absence of air injection, the TCS degradation efficiency was 71.54 ± 2.29%, which increased to 79.89 ± 3.99% upon injecting air at 1.6 Nm^3/h. The enhanced degradation can be attributed to intensified cavitation induced by dissolved air; the injected air provides heterogeneous nucleation sites, increasing the number and energy of collapsing bubbles. Thereby promoting a more efficient formation and implosion of cavitation bubbles. Moreover, the presence of air increases the partial pressure inside the bubbles, influencing the thermodynamic conditions during collapse, thus affecting the generation of reactive species, which are critical factors governing contaminant degradation efficiency[37]. On the other hand, a secondary oxidant is generated via air injection. When air is introduced into the venturi throat, pressure fluctuations facilitate the

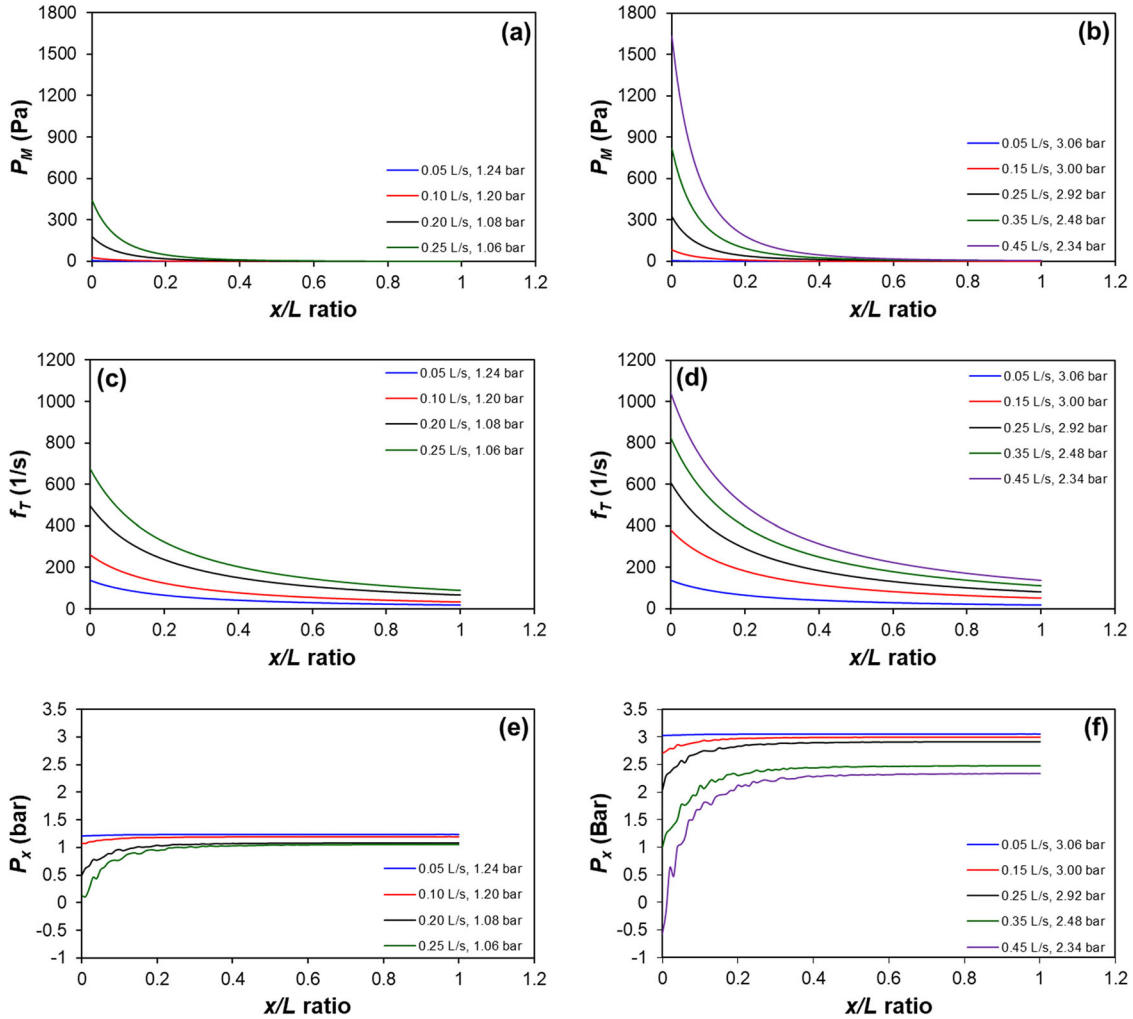

Fig. 2 | Turbulence modelling of venturi-based HC process. a, **b** Variation of turbulence frequency, **c**, **d** rate of dissipation of the turbulent kinetic energy, and **e**, **f** turbulent pressure downstream of the venturi with *x*/*L* ratio.

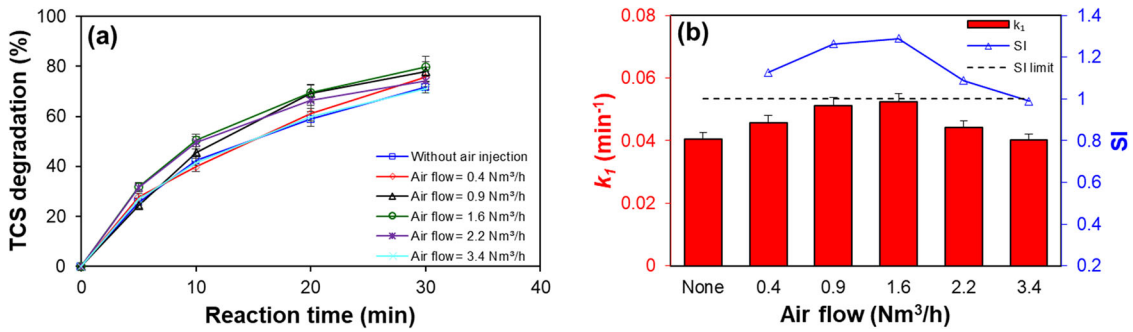

Fig. 3 | Effect of air injection flow on performance of HC process. a TCS degradation, and **b** rate constant of TCS degradation (Experimental condition: TCS concentration = 5 mg/L, solution pH = 7, inlet pressure = 2.34 bar, flow rate = 0.45 L/s, air flow rate = 0.4–3.4 Nm^3/h, and reaction time = 5–30 min).

formation of ozone (O_3), as reported in the literature and represented in Eq. (18)[38]. According to previous reports, this may initiate a cascade, producing additional reactive species such as superoxide ($O_2^{\bullet-}$) and singlet oxygen ($^1O_2$) (Eqs. 19–25)[39–41]. These secondary oxidants significantly enhance the oxidative degradation of TCS, contributing to the overall efficiency of the HC process.

However, increasing the air flow rate beyond the optimal point (1.6 Nm^3/h) to 3.4 Nm^3/h led to a decline in efficiency, dropping to 71.04 ± 2.98%. This reduction can be attributed to the complex effects of excessive aeration on the HC process, such as changes in bubble size, density, and residence time, leading to reduced generation of reactive species[40]. At very high air flow rates, larger bubbles with shorter residence times in the low-pressure zone may form, disrupting chain reactions that produce secondary oxidants and thus diminishing the overall efficiency of the aerated HC process. Furthermore, the higher air flow rate can cause choking of the venturi device due to the accumulation of excess air molecules downstream. This consequently hinders cavity cloud formation and reduces the number of cavitational events due to incomplete cavity collapses caused by gas accumulation, as noted in previous studies[20]. Additionally, excess O_2 can scavenge $^{\bullet}$OH radicals via side reactions, such as those

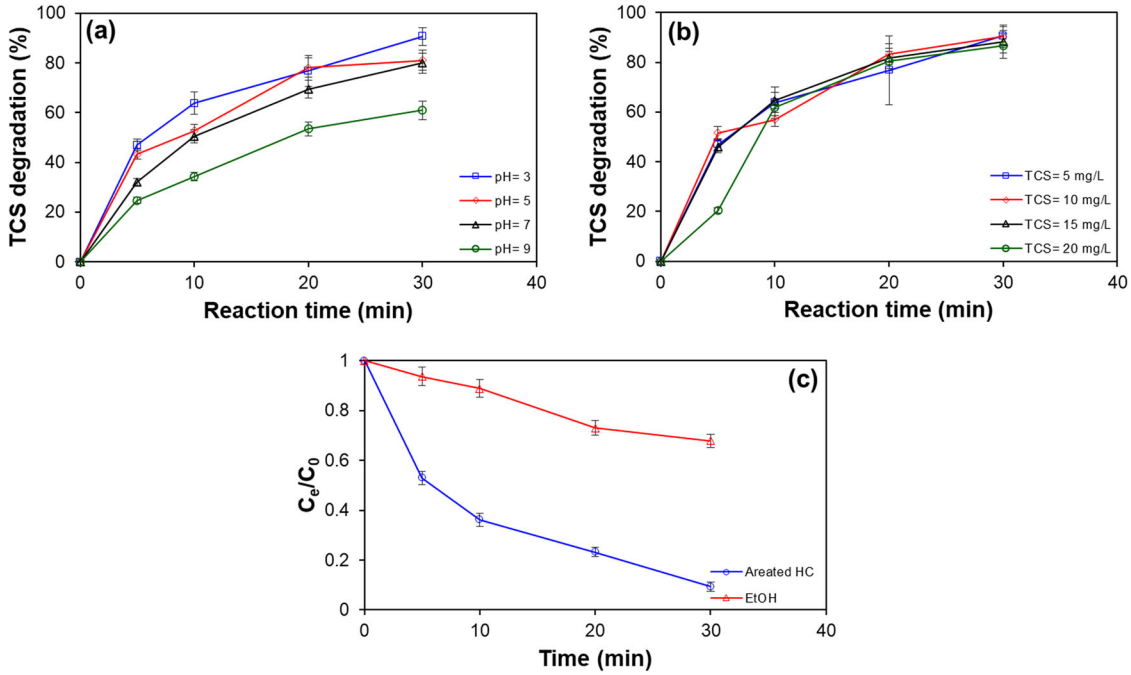

Fig. 4 | Performance of aerated HC process under various conditions. a Effect of solution pH on TCS degradation by aerated HC process (Experimental condition: TCS concentration = 5 mg/L, solution pH = 3–9, inlet pressure = 2.34 bar, flow rate = 0.45 L/s, air flow rate = 1.6 Nm^3/h, and reaction time = 5–30 min). **b** Variation of TCS degradation by aerated HC process as a function of initial TCS concentration (Experimental condition: TCS concentration = 5–20 mg/L, solution pH = 3, inlet pressure = 2.34 bar, flow rate = 0.45 L/s, air flow rate = 1.6 Nm^3/h, and reaction time = 5–30 min). **c** TCS degradation by aerated HC process under EtOH addition (Experimental condition: TCS concentration = 5 mg/L, solution pH = 3, inlet pressure = 2.34 bar, flow rate = 0.45 L/s, air flow rate = 1.6 Nm^3/h, EtOH concentration = 15 mM, and reaction time = 5–30 min).

represented by Eq. (26)[42], reducing the radicals available for TCS degradation.

$$\mathrm{Air/O_2} \rightarrow \mathrm{O_2/O_3} \quad (18)$$

$$\mathrm{O_3} \rightarrow {}^{\bullet}\mathrm{O}({}^3\mathrm{P}) + \mathrm{O_2} \quad (19)$$

$${}^{\bullet}\mathrm{O}({}^3\mathrm{P}) + \mathrm{H_2O} \rightarrow 2{}^{\bullet}\mathrm{OH} \quad (20)$$

$$2{}^{\bullet}\mathrm{OH} \rightarrow \mathrm{H_2O_2} \quad (21)$$

$$\mathrm{H_2O_2} \leftrightarrow \mathrm{H^+} + \mathrm{HO_2^-} \quad (22)$$

$$\mathrm{HO_2^-} + \mathrm{O_3} \rightarrow \mathrm{HO_2^{\bullet}} + {}^{\bullet}\mathrm{O_3^-} \quad (23)$$

$$\mathrm{HO_2^{\bullet}} \rightarrow \mathrm{O_2^{\bullet -}} + \mathrm{H^+} \quad (24)$$

$$\mathrm{O_2^{\bullet -}} + {}^{\bullet}\mathrm{OH} \rightarrow {}^1\mathrm{O_2} + \mathrm{OH^-} \quad (25)$$

$$\mathrm{O_2} + {}^{\bullet}\mathrm{OH} \rightarrow \mathrm{HO_2^{\bullet}} + \mathrm{O^{\bullet}} \quad (26)$$

To better evaluate the impact of air injection, TCS degradation data were analysed using first-order kinetics, consistent with previous studies[22]. The degradation profiles under various air flow rates fit well with the first-order model (Fig. S2), and the corresponding rate constants are summarised in Fig. 3b. The highest rate constant (0.052 ± 0.003 min^{-1}) was observed at an air flow rate of 1.6 Nm^3/h. The synergistic effect of air injection was further quantified using the synergistic index (SI), calculated from Eq. (27), where $k_{A.HC}$ and k_{HC} represent the rate constants for the aerated and non-aerated HC processes, respectively. Except for the highest air flow rate (3.4 Nm^3/h), air injection exhibited a positive synergistic effect, with the greatest enhancement at the optimal rate of 1.6 Nm^3/h. These results confirm that optimised aeration improves HC performance by intensifying cavitation and reactive oxidant production, while excessive air flow reduces efficiency due to reduced residence time and larger bubble formation.

$$\mathrm{SI} = \frac{k_{A.HC}}{k_{HC}} \quad (27)$$

Effect of solution pH and TCS concentration

To gain a deeper understanding of the aerated HC process, the impact of solution pH on TCS degradation was examined. The pH of the reaction solution was adjusted from 3 (acidic) to 9 (alkaline) while maintaining a constant initial TCS concentration of 5 mg/L. Figure 4a shows that as the solution pH increased from 3 to 9, the degradation efficiency decreased from 90.66 ± 3.54% to 60.93 ± 3.72%. The observed pH-dependent degradation efficiency can be attributed to three primary factors: oxidant generation, the molecular state of TCS, and liquid-gas interaction. Firstly, the solution pH significantly influences the generation of ˙OH radicals, a key oxidant in this process. Acidic conditions are generally favourable for ˙OH radical formation[32]. This can be explained by: (i) greater ˙OH radical availability and stability at lower pH, due to reduced scavenging by carbonate or other bases[22]; and (ii) the increased oxidation potential of ˙OH radicals in acidic solutions[43]. Consequently, variations in pH can directly impact the concentration of generated oxidants and, therefore, the overall TCS degradation efficiency.

Secondly, the molecular state of TCS is strongly dependent on the solution pH, given its pKa value of 7.68. As illustrated in the microspecies distribution curve (Fig. S3), at pH 3, TCS exists predominantly (nearly 100%) in its protonated form. The different ionic or molecular forms of TCS can exhibit varying reactivity towards the generated oxidants. The unprotonated (neutral) TCS molecule, which is dominant at a pH above 7.68, is more hydrophobic and less soluble in water than its protonated form. This hydrophobicity facilitates its diffusion and accumulation at the hydrophobic

gas-liquid interface of cavitation bubbles, where the concentration of ˙OH radicals is higher, potentially leading to enhanced degradation rates. However, the high degradation efficiency observed at pH 3, where the more hydrophilic protonated form is dominant, suggests that this effect is secondary. The primary mechanism for enhanced degradation in acidic conditions is the increased generation and reactivity of ˙OH radicals, rather than the hydrophobic interaction of the TCS molecule itself[1]. Thirdly, while the highly reactive ˙OH radicals generated during cavity collapse have a very short lifespan, limiting their diffusion into the bulk solution[32], the introduction of air into the venturi throat enhances the availability of pollutant molecules at the gas-liquid interface. This increased proximity between TCS and the generated ˙OH radicals significantly improves the probability of their interaction and subsequent degradation. Similar findings have been reported by Mishra et al.[2], who investigated TCS degradation using a rotating HC reactor with a stator-rotor arrangement. Their study showed a degradation efficiency of 35.2% at pH 2, which decreased to 7.8% at pH 10. In conclusion, solution pH plays a pivotal role in TCS degradation during the aerated HC process by influencing both the speciation of TCS and the formation and reactivity of ˙OH radicals. Understanding this pH-dependent behaviour offers key insights into the underlying mechanisms and supports the identification of optimal conditions for maximising treatment efficiency. These findings advance the development of sustainable and effective wastewater treatment strategies for removing TCS and similar contaminants from industrial effluents.

As industrial effluents often exhibit varying pollutant concentrations, understanding the performance of the aerated HC process under different initial TCS concentrations is essential for optimising its application in real-world scenarios. To assess this, the aerated HC process was tested with different initial TCS concentrations ranging from 5 to 20 mg/L, while maintaining a constant pH of 3, an inlet pressure of 2.34 bar, and a flow rate of 0.45 L/s. Figure 4b presents the TCS degradation as a function of the initial TCS concentration. As observed, increasing the initial concentration of TCS from 5 to 20 mg/L led to a slight decrease in degradation efficiency, from 90.66 ± 3.54% to 86.55 ± 4.93%. The lower degradation efficiency of the aerated HC process at higher initial TCS concentrations is likely due to the limited oxidant capacity of the process. While the total amount of pollutant increases with the initial concentration, the total concentration of ˙OH radical produced under constant operational parameters remains relatively fixed, thus leading to a decreased molar ratio of ˙OH to TCS at higher pollutant loadings[13]. This results in fewer ˙OH radicals being available per TCS molecule, consequently reducing the overall degradation performance.

To ascertain the role of ˙OH radical in the degradation of TCS by the aerated HC process, EtOH was selected as an effective ˙OH radical scavenger[44]. For the quenching experiment, 15 mM of EtOH was added to a reaction solution containing 5 mg/L of TCS at pH 3. The variation in TCS degradation by the aerated HC process in the presence and absence of EtOH is illustrated in Fig. 4c. As shown, compared to the control experiment (without EtOH), the addition of 15 mM EtOH to the reaction solution resulted in a significant inhibitory effect on TCS degradation. The degradation rate decreased from 90.66 ± 3.54% to 32.13 ± 1.61%, corresponding to a reduction in the rate constant from 0.073 min^{-1} to 0.014 min^{-1} (Fig. S4). This substantial decrease strongly indicates the dominant role of ˙OH radical in the aerated HC process. However, incomplete quenching implies the involvement of additional reactive species (e.g. $^1O_2$ and $O_2^{\bullet-}$) and pyrolytic effects in TCS degradation.

Transformation products (TPs) of TCS during the aerated HC process were identified using gas chromatography-mass spectrometry (GC-MS) analysis (Fig. S5). To enhance detection sensitivity for minor intermediates and enable accurate pathway elucidation, experiments were conducted with an initial TCS concentration of 20 mg/L under optimised conditions, including solution pH 3.0, inlet pressure 2.34 bar, flow rate 0.45 L/s, air flow rate 1.6 Nm^3/h, and reaction time 30 min. Based on the identified TPs (Figs. S6–S18) and previous studies[45–47], a comprehensive degradation pathway for TCS in the aerated HC system is proposed (Fig. 5). The degradation mechanism is primarily driven by ˙OH radical attack and proceeds through four distinct stages: (i) ether bond cleavage and dechlorination, (ii) hydroxylation, (iii) aromatic ring opening, and (iv) complete mineralisation.

The initial degradation step involves •OH-mediated cleavage of the ether bond (C–O–C) connecting the two aromatic rings in TCS. This reaction destabilises the molecular structure, yielding chlorinated phenolic intermediates that are highly susceptible to further ˙OH attack. Progressive hydroxylation and dechlorination result in the formation of polyhydroxylated derivatives, including resorcinol (indicating complete dechlorination), pyrogallol, and 1,3,5-benzenetriol. The presence of these compounds confirms the highly oxidative environment within the HC reactor. The accumulation of di- and tri-hydroxylated benzenes facilitates subsequent aromatic ring opening, yielding aliphatic carboxylic acids and esters such as decanedioic acid dimethyl ester and nonanoic acid hexyl ester. These aliphatic intermediates undergo continued oxidative fragmentation to form shorter-chain organic acids, including 2,3-dimethylbutanoic acid ester, propanoic acid, and acetic acid. The detection of citric acid suggests the degradation pathway reaches an advanced stage comparable to biological mineralisation processes[48]. Ultimately, successive carbon chain shortening leads to complete mineralisation of TCS into carbon dioxide, water, and chloride ions. Critically, no dioxin-related compounds or dimeric species, which can form from radical coupling reactions, were identified. This suggests that the high ˙OH flux and turbulent mixing in the aerated HC reactor effectively suppress recombination pathways, favouring complete oxidation instead.

Cost estimation

Despite the acknowledged importance of balancing degradation efficiency and economic costs, a systematic quantitative investigation of this trade-off is often lacking in the literature[49–51]. To bridge this gap, this paper examines cost estimation, focusing on a venturi device for capital cost assessment and subsequent trade-off analysis, building upon proposed methods in the literature[49]. In this study, a parameterised model was developed using a spreadsheet to establish a relationship between aerated HC process performance and its operating costs (Figs. S19 and S20). For these calculations, the input data from the conducted experiments and the aerated HC process setup were derived from the present work, along with specific assumptions outlined for the calculations (Table 1), based on relevant data. A detailed costing analysis for the treatment of wastewater with a total flow rate of 10 m^3/d by the aerated HC process is summarised in Table 2. As can be seen, the total annual operating cost of the proposed process was estimated at \$14.78/m^3 of treated water. While this is higher than the reported hospital treatment costs by catalytic wet air oxidation \$6.67/m^3 and by Photo-Fenton \$10.36/m^3 [52], it is significantly lower than AOP (\$23.6/m^3), a combination of biological treatment and AOPs (\$14.74/m^3), and direct incineration processes (\$61.92/m^3) used for Pharmaceutical wastewater treatment[53]. These cost differences can be attributed to factors such as the level of process scale-up and automation, the extent of mineralisation, and technology accessibility. It is important to note that real wastewaters typically contain more complex contaminant loads, potentially requiring higher investments and increasing treatment costs. Nonetheless, this cost analysis highlights the economic viability of the aerated HC process, supporting its potential for cost-effective environmental remediation.

The effective treatment of TCS-contaminated wastewater, a major pollutant among PPCPs, remains a critical challenge in environmental remediation. This study demonstrated the potential of the aerated HC process as an efficient and sustainable treatment method. Optimal degradation (90.66 ± 3.54%) was achieved at an inlet pressure of 2.34 bar, flow rate of 0.45 L/s, and pH 3 within 30 min. The short reaction time, low cost (\$14.78/m^3), and high synergistic index (SI = 1.29) highlight its feasibility for practical applications. While this study elucidates the degradation pathway for TCS, future investigations should prioritise comprehensive ecotoxicity assessments of treated effluent and associated TPs, given that oxidative degradation can generate intermediates with toxicity profiles distinct from the parent compound. Overall, the aerated HC process shows strong

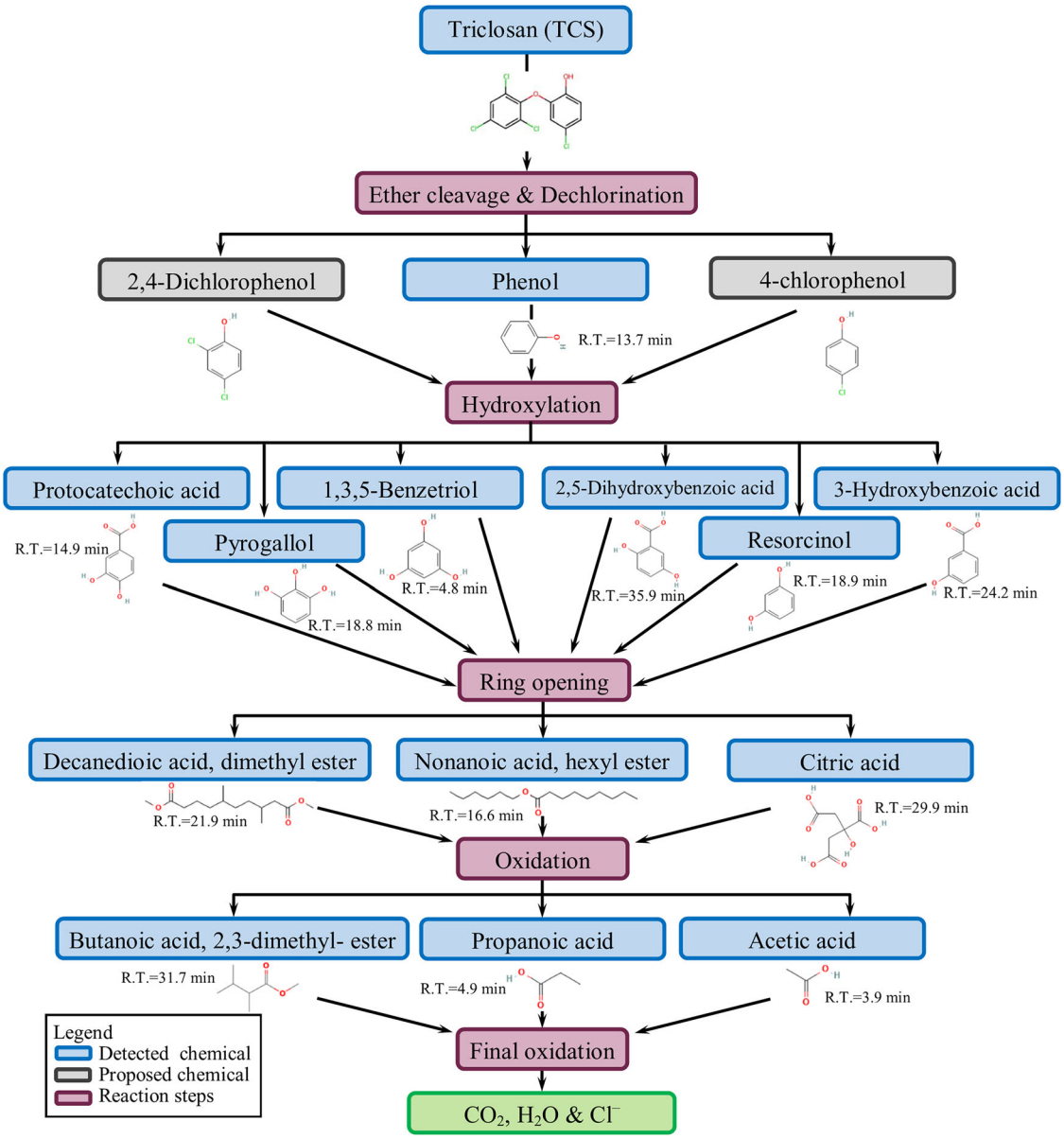

Fig. 5 | Proposed possible pathway of TCS degradation.

promise as a highly efficient and chemical-free approach for PPCP-contaminated wastewater treatment. Further research into operational optimisation and degradation pathways will support its advancement toward scalable, eco-friendly solutions

Methods

Aerated HC setup

The experiments utilised a closed-loop system featuring a venturi constriction with integrated air injection capability. A schematic diagram illustrating this process is shown in Fig. 6a. The experimental setup comprised a 50 L plastic liquid reservoir containing 8 L of working liquid. The temperature of the liquid within the reservoir was maintained at 25 ± 3 °C using a water bath throughout the experimental duration. A centrifugal pump (DYNAFLO, Model: 60061R-2, Davey Bore Master, Australia), capable of a maximum flow rate of 315 L/min and a maximum pressure of 310 kPa, was used to circulate the liquid from the reservoir through the venturi device at a controlled flow rate (Fig. S1, showing the pump's performance curve). The flow rate of the liquid was continuously monitored using a magnetic flowmeter (Yokogawa ADMAG, Model: AXF025G, China) with an accuracy of ±0.3%. To measure the pressure fluctuations within the venturi, piezoelectric pressure transducers (IFM electronic, Model PN7514, ±0.5% accuracy, Germany) were installed at distances of 10 mm upstream of the venturi inlet (P1) and 10 mm downstream of the venturi throat exit (P2). Critically, a pressurised airline was connected to a port located at the throat section of the venturi device, and the rate of air injection was measured and controlled using a rotameter (Tecfluid, Model: PTM312-0100, PTFE float, Germany) (Fig. S21). The outlet of the venturi device was connected back to the liquid reservoir, forming a closed-loop configuration that enabled continuous processing of the liquid. The circular venturi itself was constructed from stainless steel (SS316) and had the following fixed geometric parameters: an inlet diameter (D1) of 25 mm, a throat diameter (d) of 5 mm, an outlet diameter (D2) of 25 mm, a converging and diverging angle of 21.83°, and a throat length of 25 mm (Fig. 6b).

Experimental procedure

For each experimental run, a predetermined volume of 8 L of deionised water spiked with TCS was circulated through the HC process for a total duration of 30 min. During the experiments, the bypass valve was carefully adjusted to achieve the desired inlet pressure and flow rate, which was varied between 1 and 3 bar. This adjustment consequently resulted in the desired

Table 1 | Input data and assumptions for the cost estimation of the aerated HC process

Category	Items	Value	Unit
Input	Optimal inlet pressure	234,000	Pa
	Recovered pressure	20,000	Pa
	Volumetric flow rate of pump	0.00045	m^3/s
	Total volume to be treated	0.008	m^3
	Air injected flow rate	1.6	m^3/h
	Rate constant for mineralisation	0.073	min^{-1}
	Influent concentration of TCS	5	mg/L
	Required effluent concentration of TCS	0.5	mg/L
	Diameter of venturi throat	0.005	m
	Inlet pipe diameter	0.025	m
	Throat diameter: Throat length ratio	1	-
	Venturi length: Pipe diameter ratio	3	-
	Air pipe diameter	0.01	m
Assumptions	Volume of Wastewater	10	m^3/d
	Total pump efficiency	70	%
	Total compressor efficiency	70	%
	Volume occupancy in the reactor	90	%
	Pump capital cost calculation	39,358	$
	Air compressor capital cost calculation	39,358	$
	Price of electricity	0.2	$/kWh
	Price of commercial venturi (Stainless steel)	1104	$
	Diameter of commercial venturi	7.25	in
	Length of commercial venturi	32	in
	Amortised over 30 years	7	%
	Project duration	30	year
	Annual operation	52	weeks
	Weekly operation	7	days
	HCl consumption for WW pH adjustment (pH = 3)	9	L/m^3
	HCl relative density	1.49	-
	Price of HCl	150	$/ton
	Treated solution temperature change (from 30 °C to 37 °C)	7	°C
	Cold water enters (20 °C and exits at 25 °C)	5	°C
	Price of water	0.02	$/m^3$
	Sampling frequency	3	samples/ week
	Sampling labour time	1	h/sample
	O & M of treatment plan	300	h/year
	Labour cost	20	$/h
	Analysis cost	50	$/h
	Analysis time	1	h
	Part replacement cost (% of capital cost)	1	%

Table 2 | Cost estimation of aerated HC process

Category	Items	Value	Unit
General	Required time for desired removal	31.54	min
	Number of passes	106.46	
	Cost of treatment	1.27	$/m^3$
	Volumetric flow rate of pump needed	0.56	m^3/s
Venturi	Throat velocity	22.93	m/s
	Area of throat	0.02	m^2
	Throat diameter	0.18	m
	Throat length	0.18	m
	Water velocity in pipe	0.92	m/s
	Area of water pipe	0.61	m^2
	Diameter of water pipe	0.88	m
	Energy dissipation in the HC process	227,813.98	kJ
	Pump power needed	171.96	kW
	k constant	8.29	
	Water pipe diameter	34.80	in
	Total diameter of pipe	38.67	in
	Water pipe length	104.40	in
	Cost of the venturi	16,973.98	$
Air injection	Required Air flow rate	2000.00	m^3/h
	Air velocity in pipe	5.66	m/s
	Area of water pipe	0.10	m^2
	Diameter of air pipe	0.35	m
	Air compressor power needed	1.40	kW
	Cost of the Air pipe (Equal to venturi)	16,973.98	$
Capital cost	Total capital cost	112,663.96	$
	Amortised capital cost	9079.18	$
Electrical cost	Energy consumed in a year	33,174.36	kWh
	Annual electricity cost	6634.87	$
Chemicals and cooling water cost	HCl cost per year for pH adjustment	815.78	$
	Amount of water needed	0.79	m^3/s
	Water needed in a year	542,495.36	m^3
	Water cost in a year	10,849.91	$
	Total chemicals and cooling water cost	11,665.68	$
Labour cost	Annual sampling labour	156.00	h
	Total annual labour time	456.00	h
	Annual labour cost	15,960.00	$
Analytical cost	Annual analysis of labour	156.00	$
	Annual analysis cost	10,140.00	$
Part replacement cost	Annual part replacement cost	1126.64	$
Total cost	Total annual O& M cost	44,711.42	$
	Total annual operating cost	53,790.60	$
	Total water treated in a year	3640.00	m^3
	Cost of water treatment	14.78	$/m^3$

flow rate through the venturi, ranging from 0.05 to 0.43 L/s, a parameter that was continuously monitored and recorded. Several key operating parameters were systematically varied to investigate their impact on TCS degradation, including inlet pressure, which was controlled via the bypass valve and ranged from 1.15 ± 0.09 bar (low inlet pressure) to 2.76 ± 0.33 bar (high inlet pressure), flow rate (0.05–0.45 L/s), injected air flow rate (0.4–3.4 Nm^3/h), solution pH (3–9), and initial TCS concentration (5–20 mg/L). For each experimental condition, samples were collected from the liquid reservoir at predetermined time intervals (0, 5, 10, 20, and 30 min) to monitor TCS degradation over time. These samples were immediately processed and analysed using the method detailed in Section 2.4 to

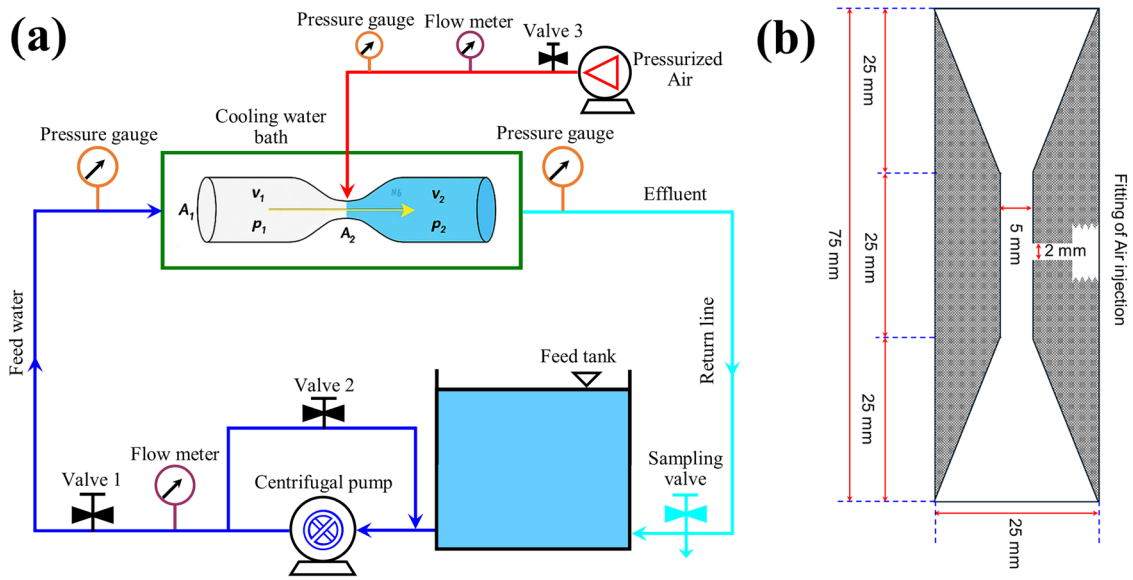

Fig. 6 | Aerated HC process setup. a Schematic diagram of the aerated HC process using a venturi device, and **b** geometry venturi device.

determine the remaining TCS concentration. In addition, to assess the role of •OH radicals in the degradation experiments, ethyl alcohol (EtOH) was added to the reaction solution at a concentration of 15 mM, and the degradation of TCS was subsequently monitored. Lastly, to assess the individual and combined effects of HC and aeration, control experiments were conducted under identical operating conditions but without the venturi device and/or without air injection.

Chemicals

Triclosan (TCS, $C_{12}H_7Cl_3O_2$, CAS#: 3380-34-5, 97.0–103.0% active substance) from Sigma-Aldrich and analytical grade acetonitrile (CH_3CN, CAS#: 75-05-8, >99.9%), sodium hydroxide (NaOH; CAS#, 1310-73-2; >98%), nitric acid (HNO_3, CAS#: 7697-37-2, >70%), ethyl alcohol (CH_3CH_2OH, CAS#: 64-17-5; >99.5%), Potassium iodide (KI, CAS#: 7681-11-0), dichloromethane (CH_2Cl_2, CAS#: 75-09-2), sodium sulphate (Na_2SO_4, CAS#: 7757-82-6), and methanol (CH_3OH, CAS#: 67-56-1) from Merck (Germany) were used as received. Stock solutions of TCS were prepared by dissolving the compound in 0.1 M NaOH and subsequently diluted with deionised water to the required working concentrations. The pH of the solutions was adjusted using 1.0 M NaOH or HNO_3 as necessary and monitored using a precalibrated multifunction pH metre (WP-90, TPS, Australia).

Analytical methods

The formation of •OH radicals along with cavitational activity during the HC process was confirmed using KI dosimetry (Supplementary Text S1). The concentration of TCS in both the treated and untreated samples was determined using high-performance liquid chromatography (UFLC, Shimadzu, Japan) equipped with a UV-Vis detector (SPD-20A, Shimadzu, Japan). Chromatographic separation was achieved using a reverse-phase C18-120 column (Shim-pack Sceptre, 150 × 3 mm, 3 µm particle size) maintained at 25 °C. The mobile phase consisted of acetonitrile and water (70:30, v/v), delivered in isocratic mode at a flow rate of 1.0 mL/min using an LC-20AD pump (Shimadzu, Japan). The detection wavelength was set at 282 nm, and the injection volume for each sample was 10 µL, with TCS eluting at a retention time of 3.77 min. Before analysis, all samples were filtered through 0.45 µm filters to remove any suspended solids[28]. Quantification of TCS was performed using a calibration curve established with standard TCS solutions in the concentration range of 0.087–10 mg/L (Fig. S22, showing the calibration curves). All measurements were performed in duplicate for each sample, and the average values (±standard deviation) were reported to ensure the reliability and reproducibility of the results.

Intermediate and by-products formed during the aerated HC process were identified using liquid-liquid extraction coupled with GC-MS[54]. In brief, reaction suspensions (100 mL) were subjected to liquid-liquid extraction using dichloromethane (3 × 10 mL) in a separatory funnel. The combined organic extracts were dried over anhydrous Na_2SO_4 and concentrated under a gentle nitrogen stream. The residue was reconstituted in methanol (1 mL), filtered through a 0.22 µm nylon syringe filter (Shanghai ANPEL, China), and stored in amber vials at −20 °C before analysis. GC-MS analysis was performed using a Shimadzu gas chromatograph (Nexis GC-2030) coupled to a Shimadzu (QP2020 NX) mass selective detector (Shimadzu Technologies, Japan). Chromatographic separation was achieved by SH-Rxi-5Sil MS capillary column (30 m × 0.25 mm i.d., 0.25 µm, Shimadzu). Sample injection (5 µL) was performed in splitless mode with an injector temperature of 250 °C. The oven temperature programme consisted of an initial hold at 50 °C for 5 min, followed by heating to 300 °C at 8 °C/min, and a final isothermal hold at 280 °C for 5 min. Helium carrier gas was maintained at a constant flow rate of 1.0 mL/min. Mass spectrometric detection was performed in electron ionisation mode (70 eV) with a scan range of m/z 40–500. The ion source and transfer line temperatures were maintained at 250 °C and 300 °C, respectively.

Data availability

No datasets were generated or analysed during the current study.

Received: 19 June 2025; Accepted: 1 September 2025;
Published online: 29 September 2025

References

1. Ren, Y.-Z. et al. Sonoelectrochemical degradation of triclosan in water. *Ultrason. Sonochem.* **21**, 2020–2025 (2014).
2. Mishra, B., Mukherjee, A., Mullick, A., Bhandari, V. M. & Moulik, S. Design of hydrodynamic cavitation assisted intensified tertiary treatment unit for effective degradation of organic micropollutants in pharmaceutical industrial effluent: a case study with triclosan. *J. Water Process Eng.* **49**, 103132 (2022).
3. Dar, O. I. et al. Source, bioaccumulation, degradability and toxicity of triclosan in aquatic environments: a review. *Environ. Technol. Innov.* **25**, 102122 (2022).
4. Pan, P., Gu, Y., Li, T., Zhou, N.-Y. & Xu, Y. Deciphering the triclosan degradation mechanism in Sphingomonas sp. strain YL-JM2C:

Implications for wastewater treatment and marine resources. *J. Hazard. Mater.* **478**, 135511 (2024).
5. Wang, F. et al. A novel cobalt-iron bimetallic hydrochar for the degradation of triclosan in the aqueous solution: performance, reusability, and synergistic degradation mechanism. *Environ. Pollut.* **358**, 124487 (2024).
6. Bhaskar, S., Apoorva, K. V., Ashraf, S. & Athul Devan, T. Synthesis and application of iron nanoparticles from scrap metal for triclosan degradation in water via Fenton and Sono-Fenton oxidation. *Waste Manag. Bull.* **3**, 293–300 (2025).
7. Moazeni, M. et al. Cobalt ferrite/MIL-101(Fe)/graphene oxide heterostructures coupled with peroxymonosulfate for triclosan degradation. *J. Water Process Eng.* **50**, 103214 (2022).
8. Thompson, A., Griffin, P., Stuetz, R. & Cartmell, E. The fate and removal of triclosan during wastewater treatment. *Water Environ. Res.* **77**, 63–67 (2005).
9. Almeida-Naranjo, C. E., Cuestas, J., Guerrero, V. H. & Villamar-Ayala, C. A. Efficient decontamination: caffeine/triclosan removal using rice husk in batch and fixed-bed columns. *Water* **16**, 197 (2024).
10. Lanjewar, S. et al. A critical review on prospects and challenges in "conceptualization to technology transfer" for nutrient recovery from municipal wastewater. *Sustainable Water Treatment: Advances and Technological Interventions,* (eds Moulik, S., Mullick, A. & Roy, A.), Wiley Online Library, 517–565 (2022).
11. Khajeh, M., Amin, M. M., Fatehizadeh, A. & Aminabhavi, T. M. Synergetic degradation of atenolol by hydrodynamic cavitation coupled with sodium persulfate as zero-waste discharge process: effect of coexisting anions. *Chem. Eng. J.* **416**, 129163 (2021).
12. Momin, R. F. & Gogate, P. R. Degradation of reactive violet 1 using innovative approach of hydrodynamic cavitation coupled with oxidants. *Chem. Eng. Sci.* **298**, 120414 (2024).
13. Jadhav, S. P. & Gogate, P. R. Intensification of hydrodynamic cavitation induced degradation of Brilliant Blue dye using various additives. *J. Indian Chem. Soc.* **102**, 101540 (2025).
14. Gągol, M., Przyjazny, A. & Boczkaj, G. Wastewater treatment by means of advanced oxidation processes based on cavitation—a review. *Chem. Eng. J.* **338**, 599–627 (2018).
15. Khajeh, M., Amin, M. M., Taheri, E., Fatehizadeh, A. & McKay, G. Influence of co-existing cations and anions on removal of direct red 89 dye from synthetic wastewater by hydrodynamic cavitation process: an empirical modeling. *Ultrason. Sonochem.* **67**, 105133 (2020).
16. Dixit, D., Thanekar, P. & Bhandari, V. M. Dual activity cavitation reactors for increased efficacy in degradation of refractory pollutants —a case study on cephalexin degradation. *Chem. Eng. Res. Des.* **192**, 310–322 (2023).
17. Han, H. et al. Synergistic enhancement in hydrodynamic cavitation combined with peroxymonosulfate fenton-like process for BPA degradation: new insights into the role of cavitation bubbles in regulation reaction pathway. *Water Res.* **268**, 122666 (2025).
18. Mohod, A. V., Teixeira, A. C. S. C., Bagal, M. V., Gogate, P. R. & Giudici, R. Degradation of organic pollutants from wastewater using hydrodynamic cavitation: a review. *J. Environ. Chem. Eng.* **11**, 109773 (2023).
19. Wang, B., Su, H. & Zhang, B. Hydrodynamic cavitation as a promising route for wastewater treatment—a review. *Chem. Eng. J.* **412**, 128685 (2021).
20. Rajoriya, S., Bargole, S. & Saharan, V. K. Degradation of reactive blue 13 using hydrodynamic cavitation: effect of geometrical parameters and different oxidizing additives. *Ultrason. Sonochem.* **37**, 192–202 (2017).
21. Wang, J. et al. Intensified degradation of textile wastewater using a novel treatment of hydrodynamic cavitation with the combination of ozone. *J. Environ. Chem. Eng.* **8**, 103959 (2020).
22. Khajeh, M., Taheri, E., Amin, M. M., Fatehizadeh, A. & Bedia, J. Combination of hydrodynamic cavitation with oxidants for efficient treatment of synthetic and real textile wastewater. *J. Water Process Eng.* **49**, 103143 (2022).
23. Azizollahi, N., Fatehizadeh, A., Pourzamani, H., Taheri, E. & Aminabhavi, T. M. Degradation of 2,4-dichlorophenol via coupling zero valent iron and hydrodynamic cavitation for sulfite activation: a turbulence modeling. *J. Environ. Manag.* **332**, 117295 (2023).
24. Dehghani, A., Baradaran, S. & Movahedirad, S. Synergistic degradation of Congo Red by hybrid advanced oxidation via ultraviolet light, persulfate, and hydrodynamic cavitation. *Ecotoxicol. Environ. Saf.* **272**, 116042 (2024).
25. Kumari, P., Ghosh, S. & Mondal, P. Hybrid process of hydrodynamic cavitation and photocatalytic oxidation for degradation of pesticides in water. *Chem. Eng. Process. Process Intensif.* **209**, 110147 (2025).
26. Song, Y., Nie, S., Ji, H., Qin, T. & Ma, Z. Degradation of methyl orange using hydrodynamic cavitation coupled with plasma oxidation and ultraviolet C. *J. Clean. Prod.* **467**, 142887 (2024).
27. Zupanc, A., Petkovšek, M., Zdovc, B., Žagar, E. & Zupanc, M. Degradation of hydroxypropyl methylcellulose (HPMC) by acoustic and hydrodynamic cavitation. *Ultrason. Sonochem.* **109**, 107020 (2024).
28. Gopalakrishnan, S., Ghosh, R., Renganathan, T. & Pushpavanam, S. Sensitive and selective determination of triclosan using visual spectroscopy. *Spectrochim. Acta Part A* **254**, 119623 (2021).
29. Wang, B. et al. Hydrodynamic cavitation and its application in water treatment combined with ozonation: a review. *J. Ind. Eng. Chem.* **114**, 33–51 (2022).
30. Azizollahi, N. et al. Hydrodynamic cavitation coupled with zero-valent iron produces radical sulfate radicals by sulfite activation to degrade direct red 83. *Ultrason. Sonochem.* **95**, 106350 (2023).
31. Gawande, G. D., Pinjari, D. V. & Chavan, P. V. Degradation of neomycin using hydrodynamic cavitation based hybrid techniques. *Chem. Eng. Process. Process Intensif.* **193**, 109543 (2023).
32. Patil, P. B., Raut-Jadhav, S., Topare, N. S. & Pandit, A. B. Combined strategy of hydrodynamic cavitation and Fenton chemistry for the intensified degradation of acetamiprid. *Sep. Purif. Technol.* **325**, 124701 (2023).
33. Chen, X. et al. Activation of persulfate with hydrodynamic cavitation in the removal of atrazine: regulating the concentration of OH and SO4− and the degradation mechanism. *J. Water Process Eng.* **65**, 105828 (2024).
34. Agarkoti, C., Gujar, S. K., Gogate, P. R. & Pandit, A. B. Pilot scale degradation of Sulfamerazine using different venturi based hydrodynamic cavitation and ultrasound reactors in combination with oxidation processes. *J. Environ. Chem. Eng.* **11**, 109857 (2023).
35. Kumar, P. S. & Pandit, A. B. Modeling hydrodynamic cavitation. *Chem. Eng. Technol.* **22**, 1017–1027 (1999).
36. Gogate, P. R. & Pandit, A. B. Engineering design methods for cavitation reactors II: hydrodynamic cavitation. *AIChE J.* **46**, 1641–1649 (2000).
37. Gogate, P. R. & Pandit, A. B. Hydrodynamic cavitation reactors: a state of the art review. *Rev. Chem. Eng.* **17**, 1–85 (2001).
38. Mahbub, P. & Duke, M. Scalability of advanced oxidation processes (AOPs) in industrial applications: a review. *J. Environ. Manag.* **345**, 118861 (2023).
39. Tao, P. et al. Synergistic effects of ultrasonic-assisted ozonation on the formation of hydrogen peroxide. *J. Environ. Chem. Eng.* **9**, 104905 (2021).
40. Lou, J., Wang, X. & An, J. Dielectric barrier discharge plasma in-situ microbubble aeration with peroxymonosulfate for levofloxacin degradation: microbubble superior performance and pH-dependent mechanism. *Sep. Purif. Technol.* **355**, 129626 (2025).
41. Bai, X. et al. Simultaneous dehalogenation and oxidation of dichloroacetamide by Cu-modified CoFe-LDH in three-dimensional continuous flow aerated electrocatalytic reactor. *Chem. Eng. J.* **500**, 156652 (2024).

42. Sivasankar, T. & Moholkar, V. S. Mechanistic approach to intensification of sonochemical degradation of phenol. *Chem. Eng. J.* **149**, 57–69 (2009).
43. Taheri, E., Fatehizadeh, A., Khiadani, M., Ghasemian, M. & Bedia, J. Application of natural hematite as catalyst in heterogeneous photo-Fenton like process for 2,4-dichlorophenol degradation. *J. Photochem. Photobiol. A* **459**, 116057 (2025).
44. Rajaei, F. et al. Enhanced removal of humic acid from aqueous solution by combined alternating current electrocoagulation and sulfate radical. *Environ. Pollut.* **277**, 116632 (2021).
45. Song, Z. et al. Efficient oxidative degradation of triclosan by using an enhanced Fenton-like process. *Chem. Eng. J.* **198-199**, 379–387 (2012).
46. Hadi, S., Taheri, E., Amin, M. M., Fatehizadeh, A. & Aminabhavi, T. M. Synergistic degradation of 4-chlorophenol by persulfate and oxalic acid mixture with heterogeneous Fenton like system for wastewater treatment: adaptive neuro-fuzzy inference systems modeling. *J. Environ. Manag.* **268**, 110678 (2020).
47. Sun, M., Zhang, Y., Kong, S.-Y., Zhai, L.-F. & Wang, S. Excellent performance of electro-assisted catalytic wet air oxidation of refractory organic pollutants. *Water Res.* **158**, 313–321 (2019).
48. Lu, Z. et al. A two-stage degradation coupling photocatalysis to microalgae enhances the mineralization of enrofloxacin. *Chemosphere* **293**, 133523 (2022).
49. Das, S., Bhat, A. P. & Gogate, P. R. Degradation of dyes using hydrodynamic cavitation: process overview and cost estimation. *J. Water Process Eng.* **42**, 102126 (2021).
50. Patil, P. B., Thanekar, P. & Bhandari, V. M. Intensified hydrodynamic cavitation using vortex flow based cavitating device for degradation of ciprofloxacin. *Chem. Eng. Res. Des.* **187**, 623–632 (2022).
51. Kore, V. S., Manjare, S. D. & Taralkar, S. V. Intensified degradation of reactive blue 222 (RB222) textile dye by a hybrid AOP system of hydrodynamic cavitation coupled with inline UV and PMS oxidant. *J. Water Process Eng.* **56**, 104472 (2023).
52. Segura, Y. et al. A comparative study among catalytic wet air oxidation, Fenton, and Photo-Fenton technologies for the on-site treatment of hospital wastewater. *J. Environ. Manag.* **290**, 112624 (2021).
53. Su, R. et al. Treatment of antibiotic pharmaceutical wastewater using a rotating biological contactor. *J. Chem.* **2015**, 705275 (2015).
54. Yang, B. et al. Oxidation of triclosan by ferrate: reaction kinetics, products identification and toxicity evaluation. *J. Hazard. Mater.* **186**, 227–235 (2011).

Acknowledgements

The authors gratefully acknowledge the School of Engineering at Edith Cowan University, Australia, for the financial support that enabled this research. Their generous contribution was instrumental in the successful completion of this study.

Author contributions

E.T. and A.F. participated in the investigation, data curation, and drafting of the manuscript. V.B. contributed to data curation and drafted the manuscript. M.K. and A.F. contributed to conceptualisation, supervision, project administration, and revising the manuscript. The final draft of the manuscript was approved by all authors for submission, and they accepted responsibility for its content.

Competing interests

The authors declare no competing interests.

Additional information

Supplementary information The online version contains supplementary material available at https://doi.org/10.1038/s41545-025-00520-z.

Correspondence and requests for materials should be addressed to Ali Fatehizadeh.